Electronic Supplementary Material (ESI) for Nanoscale.
This journal is © The Royal Society of Chemistry 2020

**Supporting Information**

# Synergistic plasmon resonance coupling and light capture in ordered nanoarray as ultrasensitive and reproducible SERS substrate

Weidong Zhao,[a,c] Yuxian Zhang,[a] Jiajia Yang,[a] Jinming Li,[a] Yun Feng,[d] Maohua Quan,*[,b] Zhou Yang*[,a] and Shuyuan Xiao*[,e,f]

[a]Department of Materials Science and Engineering, University of Science and Technology Beijing, Beijing 100083, P. R. China

[b]Institute for Advanced Materials and Technology, University of Science and Technology Beijing, Beijing, 100083, China

[c]Beijing National Laboratory for Molecular Sciences, Key Laboratory of Analytical Chemistry for Living Biosystems, Institute of Chemistry, Chinese Academy of Sciences (CAS), Beijing 100190, China

[d]Department of Ophthalmology, Peking University Third Hospital, Beijing 100191, P. R. China

[e]Institute for Advanced Study, Nanchang University, Nanchang 330031, P. R. China

[f]Jiangxi Key Laboratory for Microscale Interdisciplinary Study, Nanchang University, Nanchang 330031, P. R. China

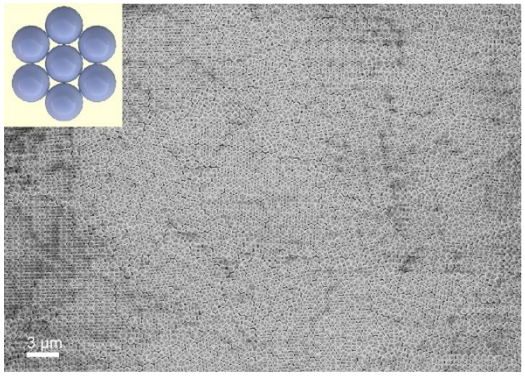


**Fig. S1.** The SEM image of large-area closely packed opal template. The inset is the schematic of structure.

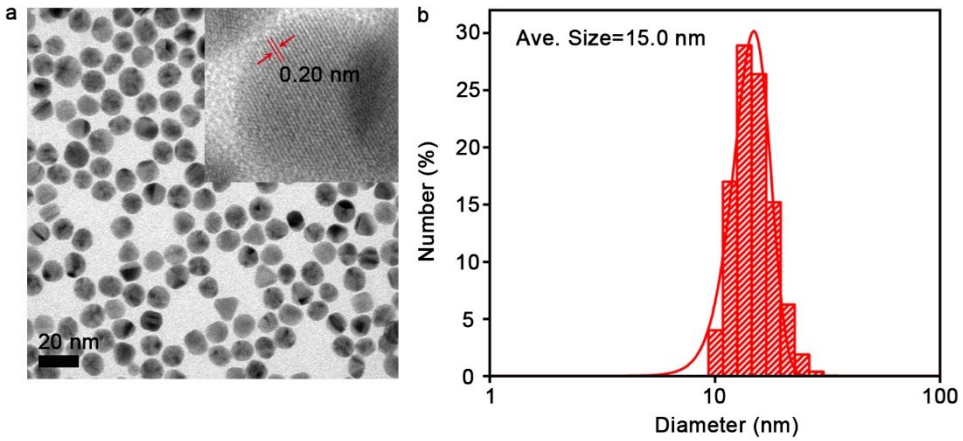


**Fig. S2.** (a) TEM image of AuNPs. The inset is HRTEM image, showing crystal planes (200) with spacing of 0.20 nm. (b) The size distribution of AuNPs with fitted normal distribution showing the average size is 15 nm.

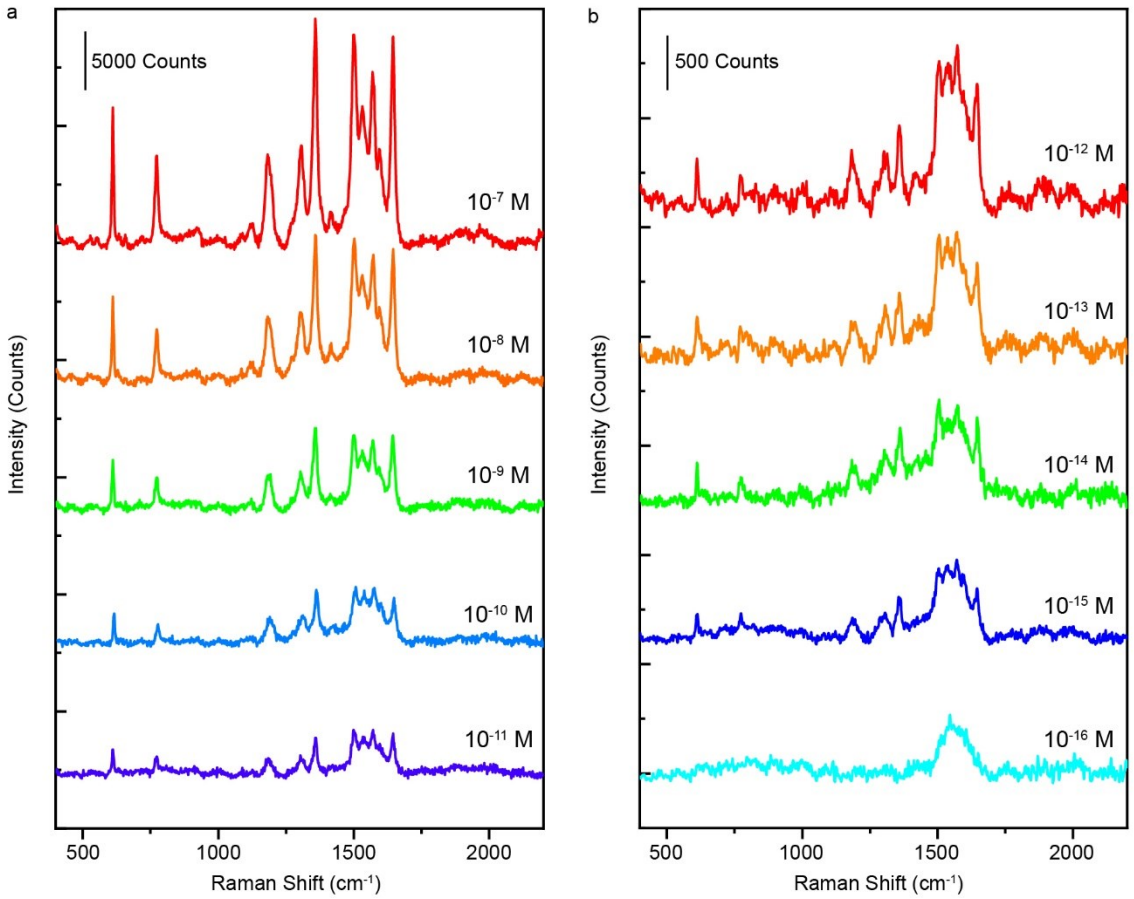


**Fig. S3.** (a,b) Raman spectra of R6G with different concentrations from $10^{-7}$ M to $10^{-16}$ M collected on PIHHN@550-100 substrate.

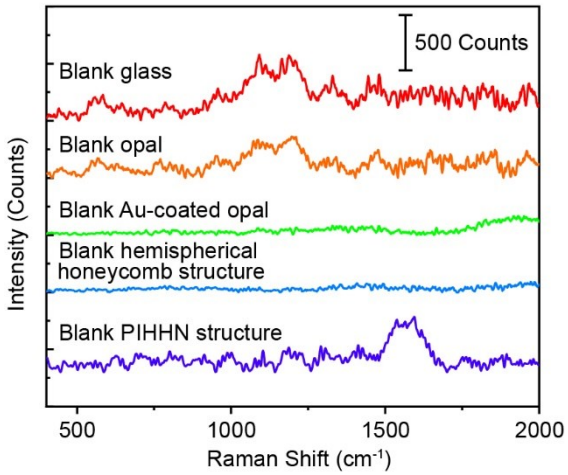


**Fig. S4** Raman spectra of blank samples collected on glass substrate, $SiO_2$ opal with diameter of 550 nm, Au-coated opal, hemispherical honeycomb structure and PIHHN@550-100 structure, respectively.

By comparing the Raman spectra for blank samples of glass substrate, $SiO_2$ opal with diameter of 550 nm, Au-coated opal, hemispherical honeycomb structure and PIHHN@550-100 structure, it can be seen that the specific peak around 1500 $cm^{-1}$ appears after adding monolayer AuNPs. Therefore, the specific peak around 1500 $cm^{-1}$ may be derived from organic matter on AuNPs surface, such as tannic acid or sodium citrate.

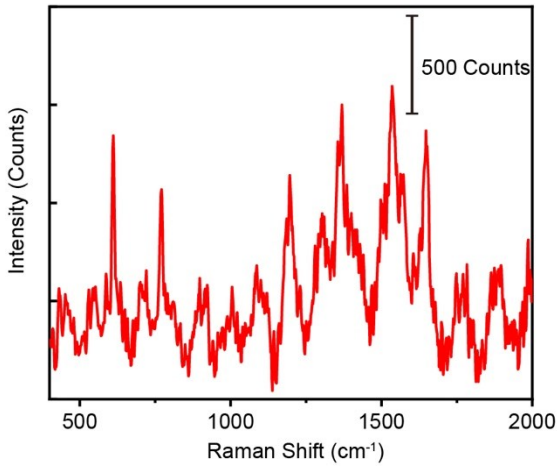


**Fig. S5.** Raman spectra of R6G at concentration of $10^{-2}$ M collected on blank glass substrate.

**The calculation of enhancement factor (EF):**

The enhancement factor (EF) of PIHHN@550-100 substrate was calculated by formula:

$$EF = \frac{I_{SERS} \times C_0}{I_0 \times C_{SERS}}$$

The $C_0$ and $I_0$ are concentration of R6G and corresponding intensity of Raman acquired on glass substrate. The $C_{SERS}$ and $I_{SERS}$ represent concentration of R6G and Raman intensity acquired on PIHHN@550-100 substrate. In this work, the $C_0$ and $C_{SERS}$ are $10^{-2}$ M and $10^{-15}$ M, respectively. The $I_0$ and $I_{SERS}$ are about 800 counts and 300 counts at specific peak of 611 $cm^{-1}$, respectively. Therefore, the EF of PIHHN@550-100 substrate is $3.75 \times 10^{12}$.

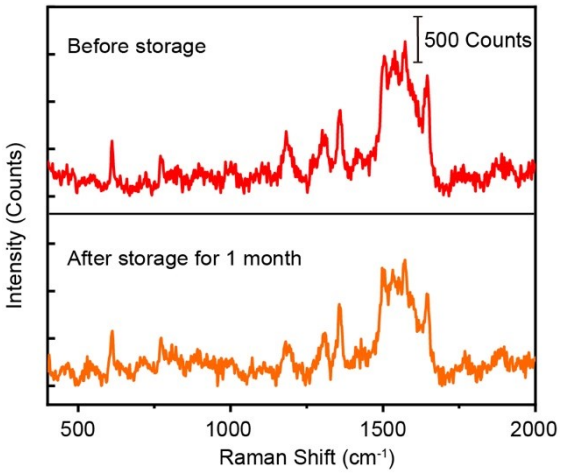


**Fig. S6.** Raman spectra of R6G at concentration of $10^{-12}$ M collected on PIHHN@550-100 substrate before and after storage for 1 month.

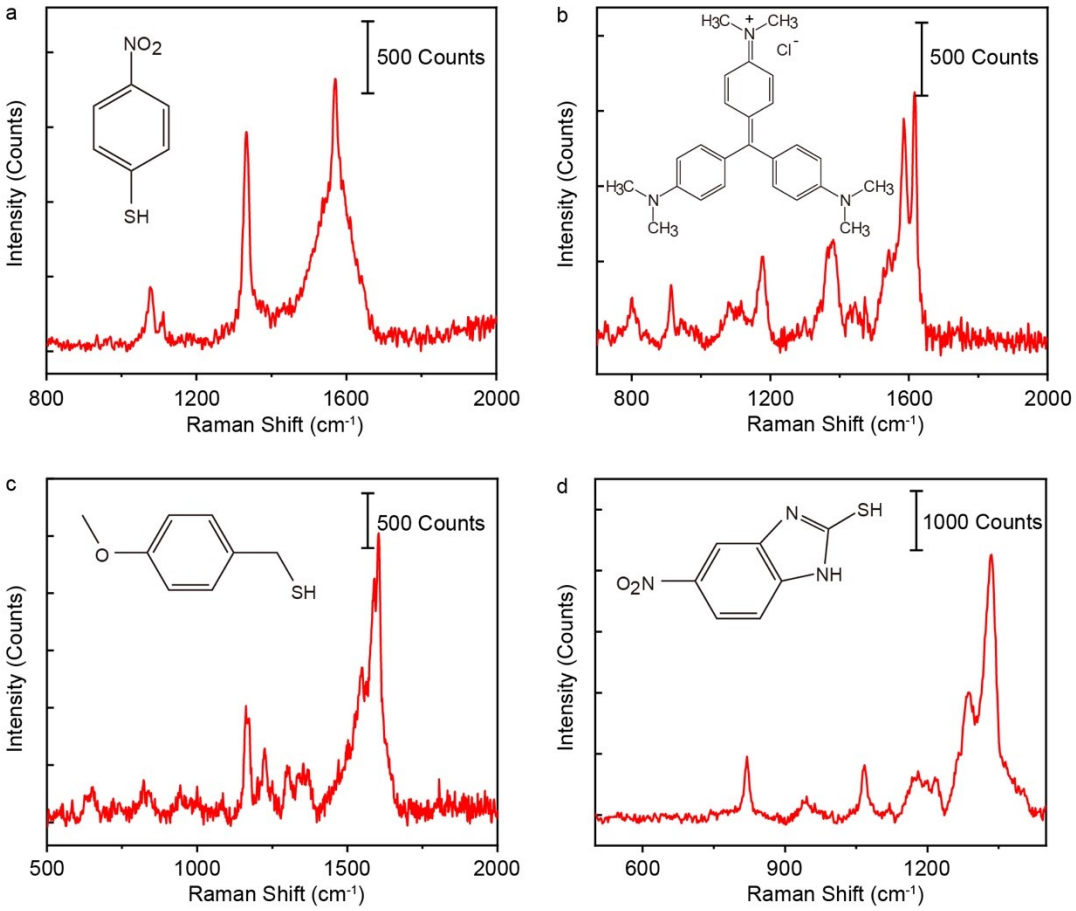


**Fig. S7.** Raman spectra of (a) 4-nitrothiophenol (4-NTP) by chemical adsorption, (b) crystal violet (CV) by physical adsorption, (c) oil soluble 4-methoxy-α-toluenethiol (MATT) and (d) water soluble 2-mercapto-5-nitrobenzimidazole (MNBI) collected on the PIHHN@550-100 substrate at concentration of $10^{-10}$ M, respectively.

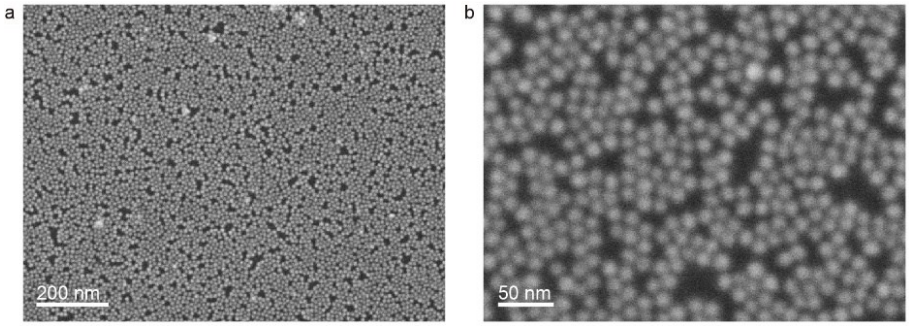


**Fig. S8.** (a) Low-magnification and (b) high-magnification SEM images of assembled monolayer AuNPs on planar substrate.

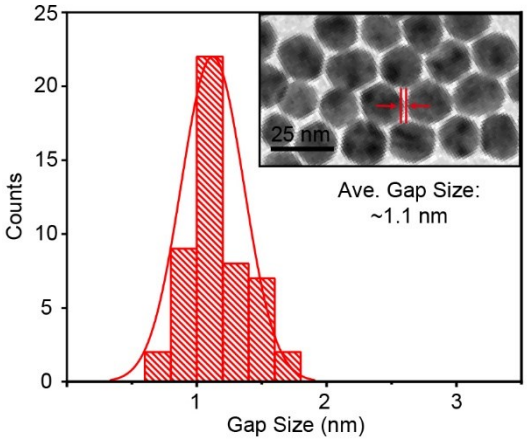


**Fig. S9.** Statistics of nanogap size between adjacent AuNPs for simulation. The inset is TEM image of assembled monolayer AuNPs on copper grid.

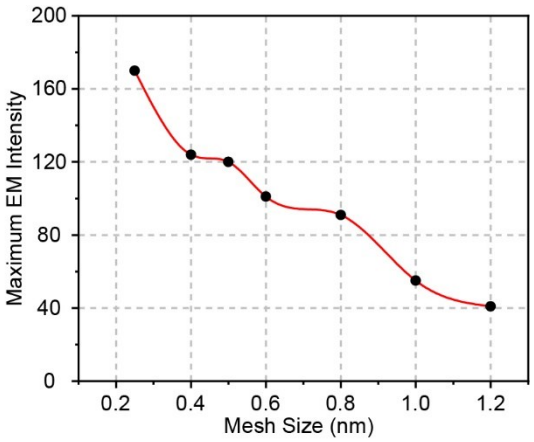


**Fig. S10.** Convergence test of FDTD simulation completed by changing the mesh size.

By observing the TEM image of AuNPs assembled on copper mesh, the average size of nanogap between adjacent AuNPs was counted to be 1.1 nm (**Fig. S9**). In addition, the convergence test of FDTD simulation was recorded by changing the mesh size, as shown in **Fig. S10**. Obviously, when mesh size reaches 0.25 nm (about 1/4 of the gap size), the EM field enhances by 160 times. However, limited by computing resources, mesh size has to increase. It can be seen that when the mesh size is 0.4 nm and 0.5 nm, the enhancement amplitude of EM field is close. Thus, the 0.5 nm mesh was adopted to release computing time.

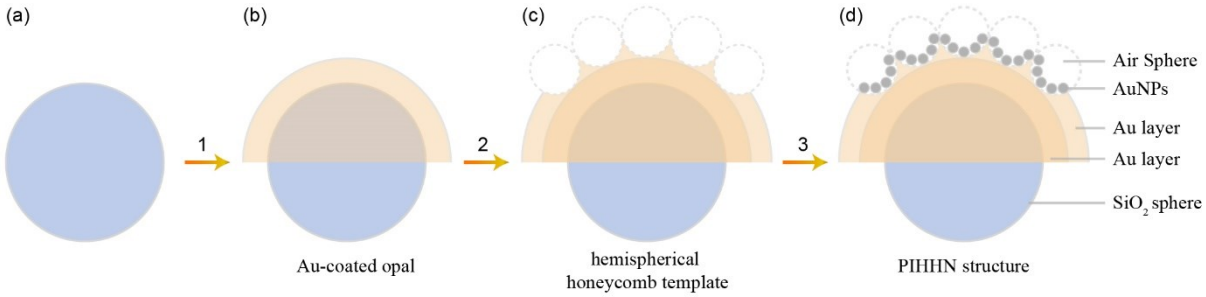


**Fig. S11.** The creation method of FDTD simulation model. 1, The Au-coated opal structure is created by covering 150 nm Au layer (mesh order of 4) on SiO2 sphere (mesh order of 3). 2, The hemispherical honeycomb template is created by again covering Au layer (mesh order of 4) and air spheres (mesh order of 2) along the circumference of Au layer. 3, The PIHHN structure is constructed by closely aligning AuNPs (mesh order of 1) along the nanocavity (air sphere).

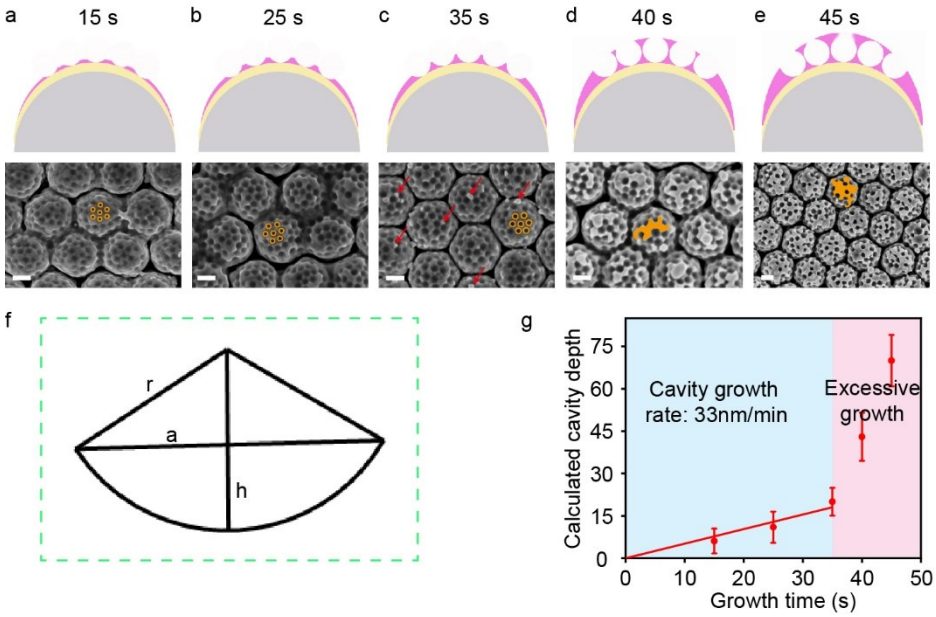


**Fig. S12.** (a-e) The schematic illustrations (top) and SEM images (bottom) showing evolution of hemispherical honeycomb structure during 1.5V at different growth time from 15 s to 45 s. The scale bar is 200 nm. (f) The geometric model for calculating the depth of nanocavity. (g) The relationship between nanocavity depth and growth time for the hemispherical honeycomb template.

The depth of metallic nanocavity was explored based on PIHHN@550-100 model under the same experimental conditions except for different electrochemical deposition times from 15 s to 45 s, as shown in **Fig. S12**. The size of nanocavity gradually increases as time goes, which is based on statistical measurement of SEM images (**Fig. S12a-e**). In particular, when the time exceeds 35 s, the large-area nanocavities are encapsulated (the yellow region in **Fig. S12d,e**). It is noted that some protrusions (indicated by red arrows) form between the nanocavities in **Fig. S12c**, which can preferentially grow and is faster than other positions, thereby covering most of the nanocavities. Further, the depth of nanocavity was accurately calculated based on the geometric model of nanocavity by formula:

$$h = r - \sqrt{r^2 - a^2}$$

where $h$ is the depth of nanocavity, $r$ is the radius of PS sphere and $a$ is the radius of nanocavity. The negative sign is chosen in that the nanocavity is thinner than the PS sphere (**Fig. S12f**). The

relationship between depth and deposition times was listed in **Fig. S12g**. When the deposition time is within 35 s, the depth of nanocavity is positively correlated with the growth time. Based on linear fitting, the growth rate is 33 nm/min. When the deposition time exceeds 35 s, the deposition state occurred mutation (considered to be excessive deposition). Therefore, this result can guide the preparation of PIHHN substrate with different sizes.

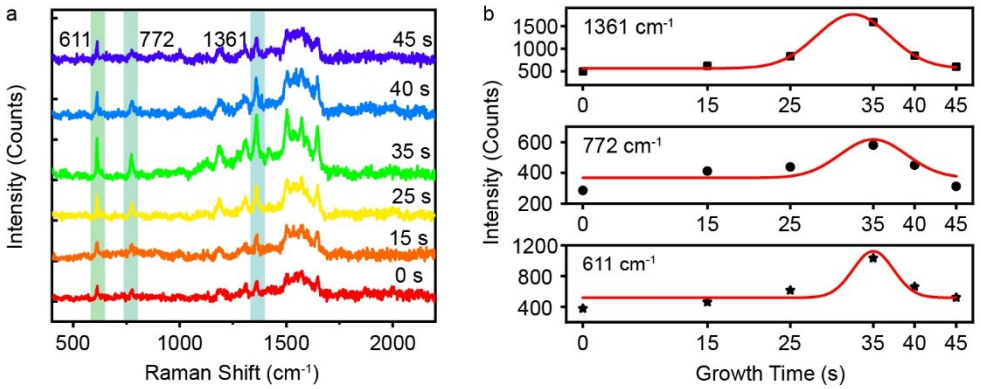


**Fig. S13.** (a) The Raman spectra of R6G collected on PIHHN@550-100 substrate at different growth times of from 0 s to 45 s, respectively. (b) Statistics of intensity deviation for Raman spectra in (a) at the specific Raman peaks of 611, 772, and 1361 $cm^{-1}$, respectively.

The Raman spectra of R6G collected on PIHHN@550-100 substrate at different deposition time from 0 s to 45 s were also recorded (**Fig. S13a,b**). It is obvious that the PIHHN@550-100 substrate corresponding to deposition time of 35 s presented the optimal SERS performance. The main reason is that perfect nanocavity array provide stronger cavity resonance to enhanced the EM field and supplied larger surface area for attachment of monolayer AuNPs to improve the density of hot spots.

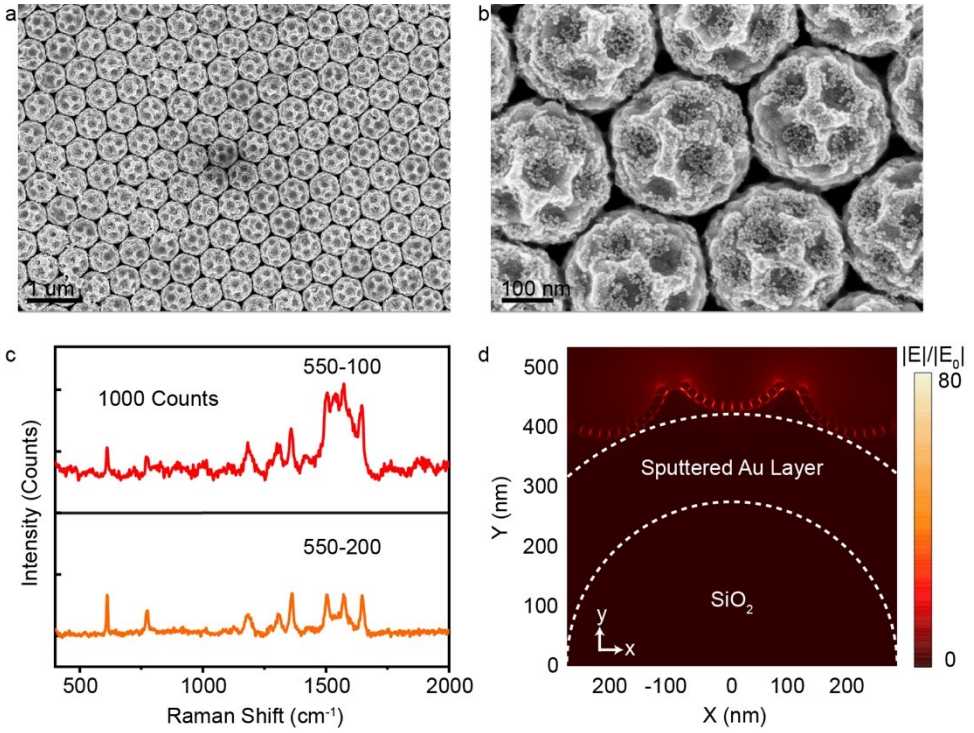


**Fig. S14.** (a,b) Low-magnification and high-magnification SEM images of PIHHN@550-200 substrate. (c) Raman spectra of R6G at concentration of $10^{-12}$ M collected on PIHHN@550-100 and PIHHN@550-200. (d) The EM field distribution excited by 633 nm laser for PIHHN@550-200 substrate.

The size of nanocavity on hemispherical honeycomb structure was regulated by altering diameter of PS microspheres under same preparation conditions except for longer deposition time, as shown in **Fig. S14**. The SEM images of PIHHN substrate based on 200 nm PS microspheres (named PIHHN@550-200) were presented to examine availability of PIHHN substrate (**Fig. S14a,b**). The Raman intensity of R6G on PIHHN@550-200 substrate at concentration of $10^{-12}$ M is slightly lower than that of PIHHN@550-100 substrate (**Fig. S14c**). In addition, the EM field distribution for PIHHN@550-200 substrate was shown in **Fig. S14d**. It can be seen that the intensity of hot spots of PIHHN@550-200 substrate ($^{|E|}/_{|E_0|}$=80) is weaker than that of the PIHHN@550-100 substrate ($^{|E|}/_{|E_0|}$=120), indicating that the increase in size of nanocavity weakens interaction with incident plane waves.

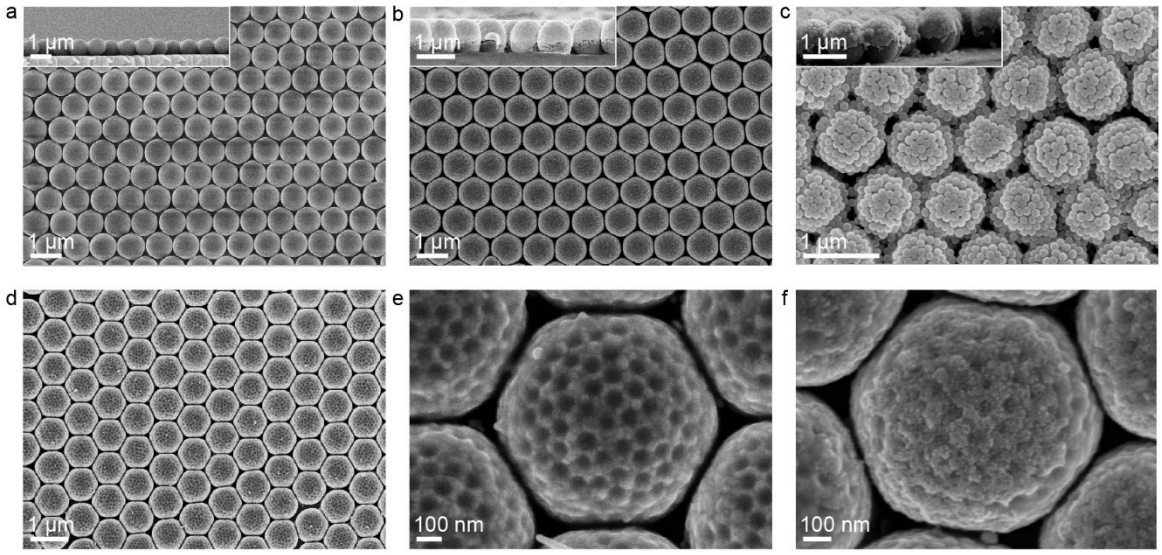


**Fig. S15.** (a-c) SEM images of 2D $SiO_2$ opal template with diameter of 800 nm, Au-coated opal template and double-layer opal template with upper layer of 100 nm PS opal, respectively. The insets represent cross-sectional SEM images of corresponding structure. (d,e) Low-magnification and high-magnification SEM images of hemispherical honeycomb template. (f) SEM image of PIHHN@800-100 substrate.

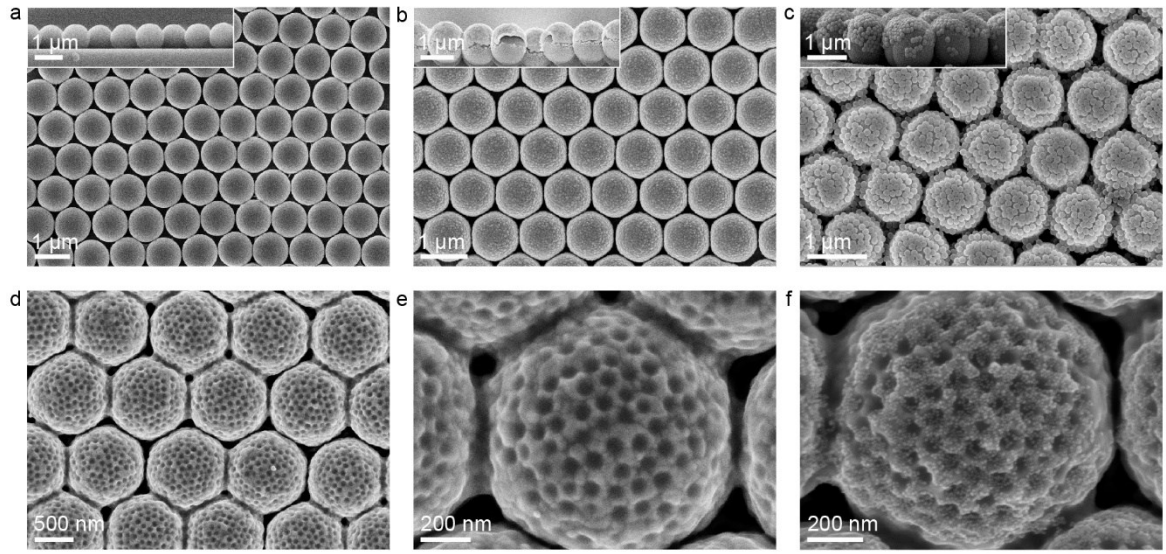


**Fig. S16.** (a-c) SEM images of 2D $SiO_2$ opal template with diameter of 1000 nm, Au-coated opal template and double-layer opal template with upper layer of 100 nm PS opal, respectively. The insets represent cross-sectional SEM images of corresponding structure. (d,e) Low-magnification and high-magnification SEM images of hemispherical honeycomb template. (f) SEM image of PIHHN@1000-100 substrate.

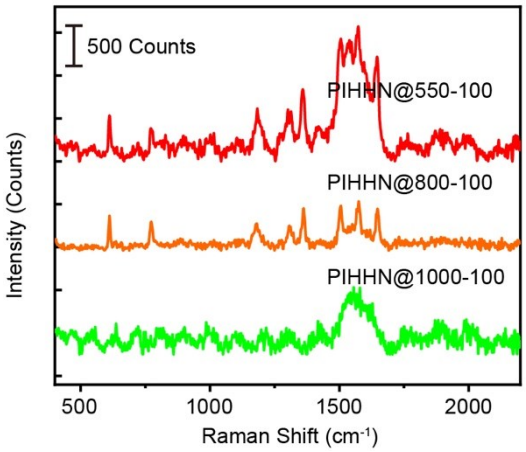


**Fig. S17.** Raman spectra of R6G at concentration of $10^{-12}$ M collected on PIHHN@550-100, PIHHN@800-100 and PIHHN@1000-100 substrate, respectively.

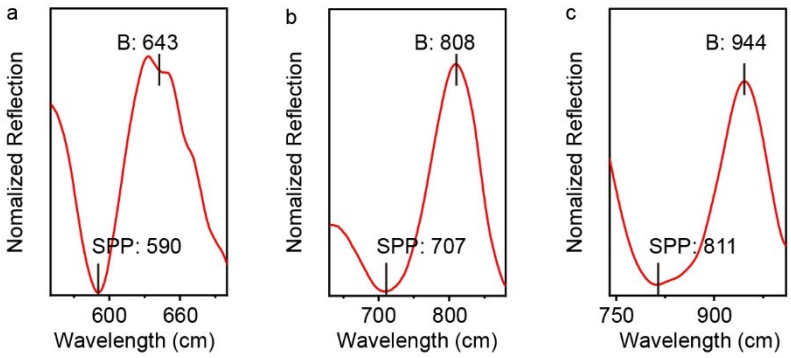


**Fig. S18.** The reflection spectra of PIHHN@550-100, PIHHN@800-100 and PIHHN@1000-100 substrate, respectively.

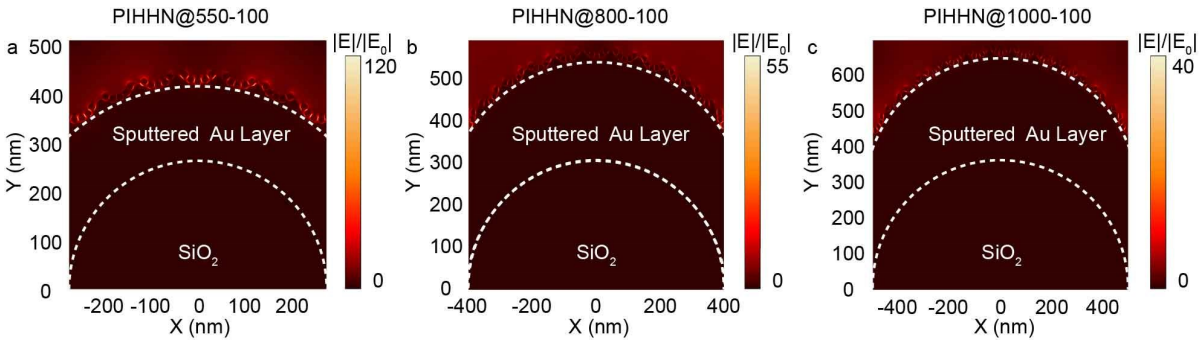


**Fig. S19.** The EM field distributions excited by 633 nm laser for (a) PIHHN@550-100, (b) PIHHN@800-100 and (c) PIHHN@1000-100 substrate, respectively.

The PIHHN substrate s constructed by $SiO_2$ microspheres with different size of 800 nm and 1000 nm were further explored under same preparation conditions (named PIHHN@800-100 and PIHHN@1000-100). The SEM images of PIHHN@800-100 and PIHHN@1000-100 were characterized in **Fig. S15** and **Fig. S16**, which demonstrate that the substrate s were successfully prepared. The Raman spectra of R6G at concentration of $10^{-12}$ M were collected on PIHHN@550-100, PIHHN@800-100 and PIHHN@1000-100 substrate, respectively (**Fig. S17**). Obviously, the Raman intensity gradually weakens as the diameter of $SiO_2$ increases. To understand the effect of diameter of $SiO_2$ microsphere on SERS performance of PIHHN substrate, we investigated the reflectance spectra and the EM field distribution excited by 633 nm laser for PIHHN@550-100, PIHHN@800-100 and PIHHN@1000-100 substrate, respectively (**Fig. S18** and **Fig. S19**). Noticeably, the SPP peak of PIHHN substrate is tunable by changing the $SiO_2$ diameter. As the diameter of $SiO_2$ sphere increases, SPP peak deviates from the laser excitation wavelength, resulting in reducing the intensity of hot spots, which is highly consistent with experimental phenomenon.

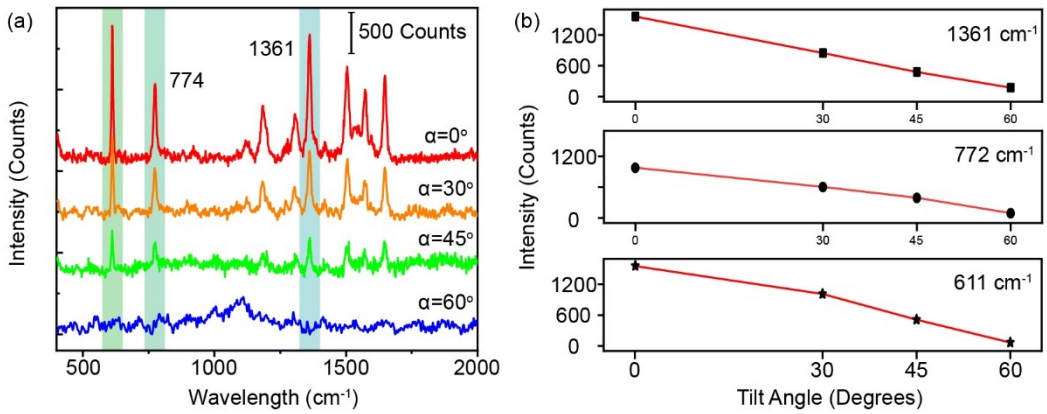


**Fig. S20.** (a) The Raman spectra of R6G at concentration of $10^{-6}$ M collected on monolayer AuNPs substrate at tilt angle from 0° to 60°. (b) Statistics of intensity deviation for Raman spectra in (a) at specific Raman peaks of 611, 772, and 1361 $cm^{-1}$, respectively.

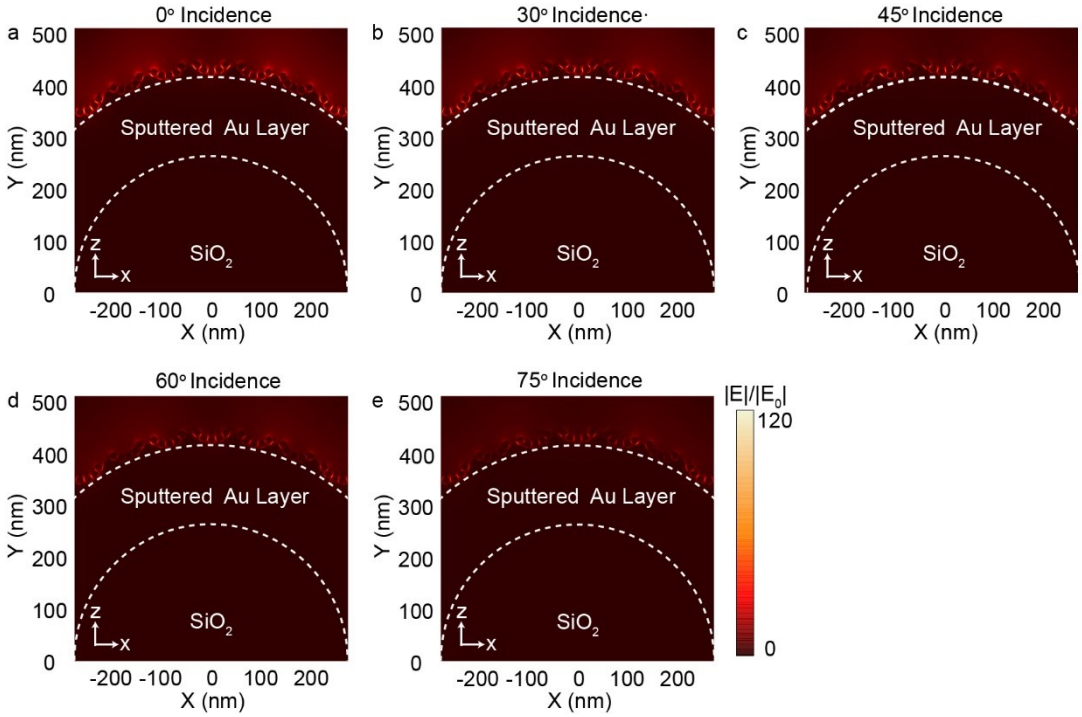


**Fig. S21.** (a-e) The EM field distributions excited by 633 nm laser for PIHHN@550-100 substrate at incident angle from 0° to 75°.

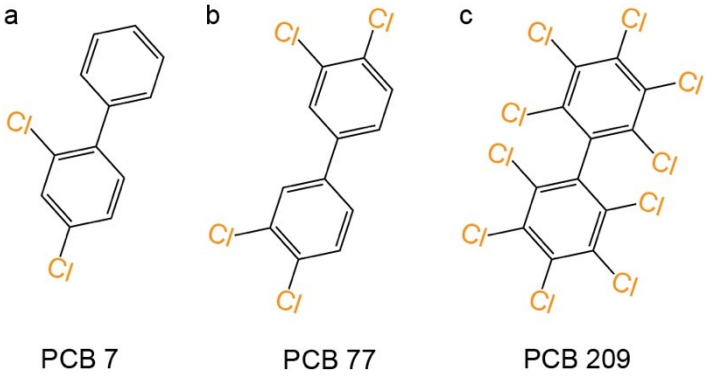


**Fig. S22.** (a-c) Molecular structures of PCB 7, PCB 77 and PCB 209, respectively.